Surface-Directed Boundary Flow in Microfluidic Channels

Tom T. Huang,[†,‡] David G. Taylor,[‡] Kwan Seop Lim,[||,⊥,#] Miroslav Sedlak,[†] Rashid Bashir,[||,⊥,+] Nathan S. Mosier,[†,§] and Michael R. Ladisch*[,§,⊥,†]

Laboratory of Renewable Resources Engineering (LORRE), School of Chemical Engineering, Department of Agricultural and Biological Engineering, School of Electrical and Computer Engineering, and Weldon School of Biomedical Engineering, Purdue University, West Lafayette, Indiana 47907, ERC for Advanced Bioseparation Technology, Inha University, Incheon 402-751, Republic of Korea, and Birck Nanotechnology Center, Purdue University, West Lafayette, Indiana 47907

Received December 22, 2005. In Final Form: March 24, 2006

Channel geometry combined with surface chemistry enables a stable liquid boundary flow to be attained along the surfaces of a 12 μm diameter hydrophilic glass fiber in a closed semi-elliptical channel. Surface free energies and triangular corners formed by PDMS/glass fiber or OTS/glass fiber surfaces are shown to be responsible for the experimentally observed wetting phenomena and formation of liquid boundary layers that are 20−50 μm wide and 12 μm high. Viewing this stream through a 20 μm slit results in a virtual optical window with a 5 pL liquid volume suitable for cell counting and pathogen detection. The geometry that leads to the boundary layer is a closed channel that forms triangular corners where glass fiber and the OTS coated glass slide or PDMS touch. The contact angles and surfaces direct positioning of the fluid next to the fiber. Preferential wetting of corner regions initiates the boundary flow, while the elliptical cross-section of the channel stabilizes the microfluidic flow. The Young−Laplace equation, solved using fluid dynamic simulation software, shows contact angles that exceed 105° will direct the aqueous fluid to a boundary layer next to a hydrophilic fiber with a contact angle of 5°. We believe this is the first time that an explanation has been offered for the case of a boundary layer formation in a closed channel directed by a triangular geometry with two hydrophobic wetting edges adjacent to a hydrophilic surface.

Introduction

Microfluidic devices are characterized by low sample intake, nanoliter volumes, and minimal reagent consumption.[1−4] Surface forces may play a dominant role in the formation of boundary layers of liquids at an air−liquid interface in microscale devices. Microscale liquid wetting phenomena have been studied extensively principally on open channel systems that provide a ready air−liquid interface.[5−11]

Zhao et al. achieved surface-directed liquid flow by patterning surfaces with different free energies inside an enclosed rectangular microchannel.[12−14] Multi-stream laminar flow or photolithography based on self-assembled monolayer (SAM) chemistry was used to obtain these patterns. Hibara et al. developed a capillarity restricted modification method for producing gas−liquid two-phase flow inside of a microchannel,[15] while Huh et al. demonstrated that an air−liquid two-phase flow generates 15−100 μm wide liquid sample streams inside of an enclosed hydrophobic microchannel.[16] These results suggest microfluidic flow inside an enclosed microchannel system can be manipulated by surface wettability, thus complementing capillary,[17] chemical,[18] electrical,[19] mechanical,[20] and optical[21] control methods by providing a nonmechanical means to position and control fluids in practical microchannel applications.

Surface chemistry positions the fluid next to the fiber due to the unique geometry of microfluidic channels with low corner angles and an elliptical cross-section causing the formation of a liquid boundary layer inside of the closed microchannel. This configuration has been used to hydrodynamically focus cells in a boundary flow for purposes of counting them.[4] This paper presents mechanisms responsible for the surface wetting phenomena observed experimentally in microfluidic devices fabricated by placing a hydrophilic glass fiber between surfaces of hydrophobic poly(dimethylsiloxane) (PDMS) and hydrophobic octadecyltrichlorosilane (OTS) on a silicon wafer or glass slide surface and pressing them together to form elliptically shaped, 100 μm wide microchannels with a 12 μm apex.[4] Geometry and

* Corresponding author. Phone: (765) 494-7022. Fax: (765) 494-7023. E-mail: ladisch@purdue.edu.
[†] LORRE, Purdue University.
[‡] School of Chemical Engineering, Purdue University.
[§] Department of Agricultural and Biological Engineering, Purdue University.
[||] School of Electrical and Computer Engineering, Purdue University.
[⊥] Weldon School of Biomedical Engineering, Purdue University.
[#] Inha University.
[+] Birck Nanotechnology Center, Purdue University.

(1) Stone, H. A.; Kim, S. *AIChE J.* **2001**, *47*, 1250.
(2) Khandurina, J.; Guttman, A. *J. Chromatogr., A* **2002**, *943*, 159.
(3) Meldrum, D. R.; Holl, M. R. *Science* **2002**, *297*, 1197.
(4) Huang, T. T.; Taylor, D. G.; Sedlak, M.; Mosier, N. S.; Ladisch, M. R. *Anal. Chem.* **2005**, *77*, 3671.
(5) Chaudhury, M. K.; Whitesides, G. M. *Science* **1992**, *256*, 1539.
(6) de Crevoisier, G.; Fabre, P.; Corpart, J.-M.; Leibler, L. *Science* **1999**, *285*, 1246.
(7) Gau, H.; Herminghaus, S.; Lenz, P.; Lipowsky, R. *Science* **1999**, *283*, 46.
(8) Kataoka, D. E.; Troian, S. M. *Nature* **1999**, *402*, 794.
(9) Ichimura, K.; Oh, S.-K.; Nakagawa, M. *Science* **2000**, *288*, 1624.
(10) Lahann, J.; Mitragotri, S.; Tran, T.-N.; Kaido, H.; Sundaram, J.; Choi, I. S.; Hoffer, S.; Somorjai, G. A.; Langer, R. *Science* **2003**, *299*, 371.
(11) Seemann, R.; Brinkmann, M.; Kramer, E. J.; Lange, F. F.; Lipowsky, R. *Proc. Natl. Acad. Sci. U.S.A.* **2005**, *102*, 1848.
(12) Zhao, B.; Moore, J. S.; Beebe, D. J. *Science* **2001**, *291*, 1023.
(13) Zhao, B.; Moore, J. S.; Beebe, D. J. *Anal. Chem.* **2002**, *74*, 4259.
(14) Zhao, B.; Moore, J. S.; Beebe, D. J. *Langmuir* **2003**, *19*, 1873.
(15) Hibara, A.; Iwayama, S.; Matsuoka, S.; Ueno, M.; Kikutani, Y.; Tokeshi, M.; Kitamori, T. *Anal. Chem.* **2005**, *77*, 943.
(16) Huh, D.; Tung, Y.-C.; Wei, H.-H.; Grotberg, J. B.; Skerlos, S. J.; Kurabayashi, K.; Takayama, S. *Biomed. Microdevices* **2002**, *4*, 141.
(17) Juncker, D.; Schmid, H.; Drechsler, U.; Wolf, H.; Wolf, M.; Michel, B.; de Rooij, N.; Delamarche, E. *Anal. Chem.* **2002**, *74*, 6139.
(18) Gallardo, B. S.; Gupta, V. K.; Eagerton, F. D.; Jong, L. I.; Craig, V. S.; Shah, P. R.; Abbott, N. L. *Science* **1999**, *283*, 57.
(19) Pollack, M. G.; Fair, R. B.; Shenderov, A. D. *Appl. Phys. Lett.* **2000**, *77*, 1725.
(20) Unger, M. A.; Chou, H. P.; Thorsen, T.; Shere, A.; Quake, S. R. *Science* **2000**, *288*, 113.
(21) Liu, G. L.; Kim, J.; Lu, Y.; Lee, L. P. *Nat. Mater.* **2006**, *5*, 27.

10.1021/la053465h CCC: $33.50 © 2006 American Chemical Society
Published on Web 06/08/2006

surface forces, modeled using FLUENT (Fluent Inc., Lebanon, NH) software, explain the boundary layer formation as a function of surface free energy of the device's surfaces and the elliptical geometry of the closed channel. Modeling also shows that analogous phenomena will occur for triangular channels, but not for rectangular ones. Rectangular channels have a constant radius of curvature and constant liquid−air interfacial area across the cross-section of the channel, thus preventing boundary layer formation due to a surface tension difference. We believe this is the first time that an explanation has been offered for the case of boundary layer formation directed by a corner with an angle of less than 90°, that is, a triangular geometry with two hydrophobic edges adjacent to a hydrophilic one.

Materials and Methods

Microdevice Fabrication and Visualization. The fabrication of a press-fit device capable of producing a microfiber-directed boundary layer follows the procedure described by Huang et al.[4] Briefly, a glass fiber (12 μm in diameter and either 4 or 10 mm in length) is sandwiched between a 1 mm-thick poly(dimethylsiloxane) (PDMS) film and a hydrophobic octadecyltrichlorosilane (OTS)-modified SiO_2 wafer. This creates a microchannel that follows the glass fiber surface and has an elliptical cross-section with a half-width of between 80 and 120 μm, depending on how the device is fabricated. A glass fiber from glass wool (obtained from Purdue University Chemistry Stores) was pulled from the wool using tweezers. On the basis of measurement using an optical microscope, a CCD camera, and a 10 μm calibrated grid manufactured by Bausch & Lomb (Rochester, NY), the average diameter of 10 strands of the glass fiber is determined to be 12 ± 0.5 μm. Visual inspections of the fibers were used to select those that were sufficiently straight and of a suitable length for constructing microchannels. Fibers were cleaned by ultrasonication in absolute ethanol for 5 min. The contact angle of the curved glass fiber surface is difficult to measure directly. The contact angle of the glass fiber for purposes of modeling was chosen to be 5°, because a glass slide, cleaned with absolute ethanol, gives a contact angle of 5−10°.

The PDMS was made from a Dow Corning Sylgard 184 silicone elastomer kit with a ratio of 10:1 elastomer base/curing agent. The contact angle of the PDMS varied from 89° to 110° and depends on the curing condition, composition, and additives. Using a punch, a sample well and an outlet port were created in the PDMS film, and these ports were completed when the film was pressed onto a wafer or glass slide.[4] Tubing (Platinum-cured silicone 0.64 mm o.d., 0.30 mm i.d. Catalog no. C-96115-00 Cole-Parmer, Vernon Hill, IL) placed in the outlet hole and glued using uncured PDMS connects the outlet port to a 50 mL syringe, which serves as a vacuum source while the sample well remains at ambient atmospheric pressure. A vacuum sufficient for atmospheric pressure on the sample well to push fluid through the device at a rate of 15 ± nL/min is obtained by manually pulling back on the syringe plunger to create a vacuum measured by a vacuum gauge (Catalog no. C-68004-00, 30-0 in. Hg, Cole-Parmer, Vernon Hill, IL) connected to the 0.64 mm o.d. tubing by a Tee fitting (Catalog no. U-433, Upchurch Scientific, Oak Harbor, WA). The fluid itself was deionized water. The modification of SiO_2 wafer (⟨100⟩ Wafer World, West Palm Beach, FL) surface with OTS was carried out as described by Huang et al.[22] The contact angle was 105−110°, as measured by a Ramé−Hart contact angle goniometer (model #100-00, Ramé−Hart Instrument Co., Netcong, NJ).

This fabrication technique is referred to as "press-fit" because the flexible PDMS film is pressed onto the inflexible OTS-coated wafer causing the film to fit around the fiber. The PDMS adheres to the OTS surface, forming an elliptically shaped channel with a liquid-tight seal around the fiber. Microfiber-directed boundary layers are observed in press-fit microdevices by pipetting a volume of 1 μL

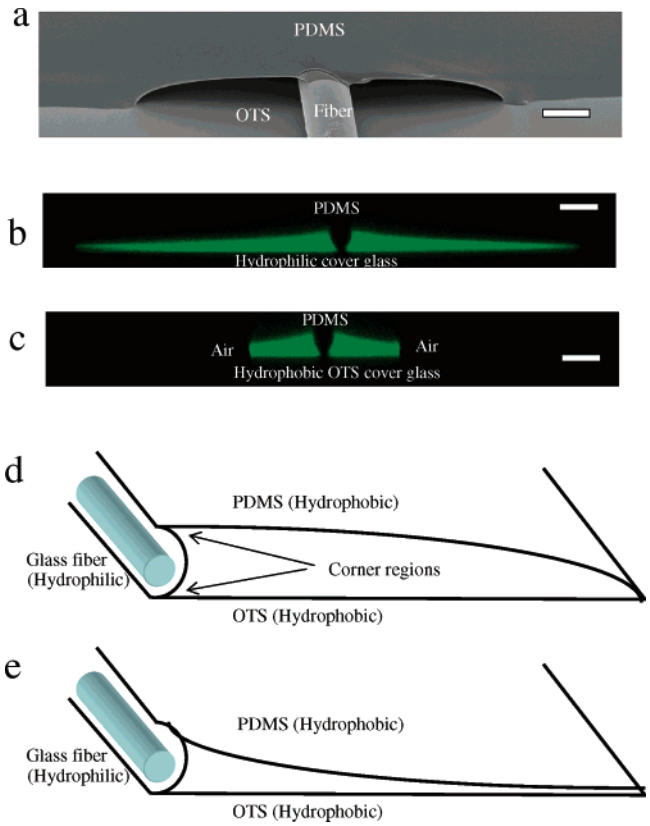

Figure 1. (a) Scanning electron microscopy (SEM) image shows (a) cross-sectional view of a press-fitted microchannel with dimensions of 12 × 88 μm under ambient conditions (conditions given in text, scale bar of 12 μm). Confocal image of press-fit microdevice filled with 1 mg/mL FITC under 127 mmHg vacuum on (b) a hydrophilic cover glass and (c) a hydrophobic OTS-modified cover glass (conditions given in text, scale bar is 20 μm). (d) Schematic illustration of the elliptical-shaped microchannel showing location of triangular corner regions, and (e) schematic illustration of the elliptical-shaped channel that is in a rotational symmetry from (d). (Drawings are not to scale.)

water into the sample well and drawing it through the device by pulling a vacuum (127 mmHg) at the outlet. Sufficient adhesion to form a tight liquid seal under pressure is achieved when either one or both surfaces are hydrophobic. Evaporation, associated with the gas−liquid interfaces and the use of vacuum to produce pressure-driven flow that pushes liquid through the device in a continuous manner, is less than 0.05% of the volume of fluid flowing through the device. We calculated this value assuming isothermal conditions and vapor/liquid equilibria.[4] In actual practice, water loss may be larger than 0.05% because PDMS is a porous polymeric material that can adsorb small amounts of water under such conditions.

The particular device used in this work has wells that are open to the atmosphere. The atmospheric pressure at the sample well pushes the liquid from the well along the flow path toward the lower pressure region at the outlet. For a single channel device, the air left within the channel at partial vacuum is a stagnant layer. For a multichannel device, air flows in from one sample well, and water from the other.[4] In either case, the air itself forms a boundary layer that is trapped between surfaces of a device that has hydrophobic surfaces. In the cases discussed in this paper, the air is adjacent to the liquid layer and results in the liquid phase flowing through the device, with a stagnant layer of air trapped inside the device.

Scanning electron microscopy (Figure 1a) showing the cross-section of the microchannel was carried out on a JEOL JSM-840 via sputter coating with Au/Pd. The magnification was 750× at 5 kV. Confocal microscopy of press-fit devices filled with 1 mg/mL FITC (fluorescein isothiocyanate) in deionized water was performed using a Bio-Rad (Hercules, CA) Radiance 2100 MP Rainbow System. To obtain better confocal images, a thin cover glass (No. 1, 130−

(22) Huang, T. T.; Geng, T.; Akin, D.; Chang, W.-J.; Sturgis, J.; Bashir, R.; Bhunia, A. K.; Robinson, J. P.; Ladisch, M. R. *Biotechnol. Bioeng.* **2003**, *83*, 416−427.

170 μm in thickness, Catalog no. 48404-143, VWR, South Plainfield, NJ) was used as substrate instead of OTS-modified SiO_2 wafer (suggested by Jennifer Sturgis of the Purdue University Flow Cytometry Laboratory). The cover glass was either modified with OTS using techniques described above to achieve hydrophobic surfaces or ultrasonically cleaned in ethanol to render the surface hydrophilic. While holding a vacuum at 127 mmHg at the device outlet, the cross-section of the boundary layer containing FITC was scanned through a 40× /1.30 N.A. oil immersion objective with an argon laser (blue) at 488 nm wavelength. The FITC fluorescence emission was directed to a high sensitivity photon multiplier tube (PMT) whose signal was acquired by Bio-Rad LaserSharp 2000 software and displayed as an image.

Confocal microscopy shows the liquid (light color in Figure 1b) completely fills the microchannel formed by the sandwich of a 12 μm glass fiber between PDMS and a hydrophilic cover glass, resulting in single phase flow. On the other hand, formation of fluid boundary layers around the glass fiber (Figure 1c) is achieved when the hydrophilic cover glass is replaced by a hydrophobic OTS-modified cover glass. The boundary layer is 35 μm in width measured from the outer edge of the fiber. These observations, as well as visual microscopy[4] showing the formation of boundary layers, led to the question of how surfaces with different hydrophobic character might be used to control the width and thickness of boundary layers flowing through a microfluidic device.

The system in which a fiber is placed between OTS and PDMS is ideal for rapid assembly of devices that begin to address how materials with defined hydrophobic character may be used to control boundary layer flow. This construction technique results in an elliptical cross-section that provides a novel approach to shaping microfluidic flow. Computational fluid dynamic simulation was carried out to better understand how such devices might be devised to function in a predictable manner.

Computational Fluid Dynamic Simulation. Computational fluid dynamic simulations were carried out using FLUENT 6.0's volume of fluids (VOF) model. The model allows unsteady transient tracking of the interface between the air and liquid. In our case, a single set of momentum equations is shared by two fluids (i.e., air and water), and the volume fraction of each fluid in each cell is tracked by solution of continuity equations for the volume fraction of one (or more) phase. The VOF model used in this study includes the effect of surface tension along the interface between air and liquid. The wall adhesion effect is also included in the model. It imposes the boundary condition at the surface. The surface tension and wall adhesion model in FLUENT uses the continuum surface force model proposed by Brackbill et al.[23] Detailed mathematical descriptions of the model are available as Supporting Information.

Using the model provided by FLUENT, the position of the air liquid interface may be tracked after application of initial boundary conditions, which include the microchannel geometry and dimensions (elliptical geometry with 12 μm fiber (minor axis) and 100 μm channel opening (major axis)), surface tension parameters of the liquid phase (water, 0.1 N/m), and, most importantly, the wetting angles at walls. We refer to a surface as hydrophobic where the liquid (water) wetting angle is 90° or higher and hydrophilic where the wetting angle is less than 45°. Simulations may be performed in either two or three dimensions, and for transient or steady wetting behaviors inside a microchannel with predefined surface free energies. This paper presents results for both transient and steady-state behavior. The solution illustrates the impact of triangular corners on microfluidic boundary layer formation.

Results and Discussion

The development of a microfiber-directed boundary layer follows two general stages. The first stage is preferential corner wetting of the microchannel regions formed by PDMS/glass fiber and OTS/glass fiber that initiates the boundary layer formation. The second stage is the subsequent wetting of microchannel walls formed by PDMS and OTS surfaces along the length of the glass fiber, which stabilizes the boundary layer. For both stages, geometry and surface chemistry control the wetting.

Stage One: Initial Corner Wetting. The development of the microfiber-directed boundary layer is controlled by the initial wetting behavior at the microchannel entrance, and particularly the corner regions formed by PDMS/glass fiber and OTS/glass fiber. These corner regions arise from the elliptical geometry of the press-fit device (Figure 1a, d, and e). The channels are symmetric along the length of the fiber, and hence the symmetrical representations of Figure 1d and e are used for the model. While Figure 1d is useful in describing the channel geometry under ambient pressure, Figure 1e describes the channel under 126 mmHg vacuum where the deformation of PDMS produces a geometry that is in a rotational symmetry from Figure 1d, and consistent with the confocal image of Figure 1b. We use both geometries to model the wetting phenomena inside of the press-fit microchannel.

Figure 2 illustrates different possibilities of static corner wetting of water in rectangular (Figure 2a−d, left panels), triangular (middle), and elliptical microchannels (right side of Figure 2). In the case where all surfaces are hydrophobic, a boundary layer will not form (Figure 2a). Surface wettability at microchannel walls is a function of the locations of the hydrophobic or hydrophilic surfaces. The boxed selection in Figure 2c corresponds to the experimental configuration shown in Figure 1c that illustrates boundary layer formation next to the fiber. The hydrophilic glass fiber surface adjoins hydrophobic PDMS and hydrophobic OTS surfaces to form an elliptical microchannel. Air buffers the liquid flow against filling a channel consisting of two adjacent, hydrophobic surfaces (Figure 2c).

For static wetting of a liquid between two surfaces, the minimization of surface area of a liquid may result in a curved interface. In the curved wetting interface (Figure 3a and b) created by liquid (water) wetting a corner, the pressure on the concave side (air for this case) is higher than the pressure on the convex side (liquid water). This relationship is described by eq 1, the Young−Laplace equation,[24]

$$\Delta P = \gamma(1/R_1 + 1/R_2) \tag{1}$$

where ΔP is the pressure difference, γ is the liquid surface tension, and R_1 and R_2 are the radii of curvature in directions perpendicular and parallel to the liquid stream.

The initial wetting behavior of a wetting liquid (water) at a corner under ambient conditions is a function of both the geometry and the surface free energies of the microchannel. The radius of curvature R, corner angle ϕ, arc length h, and wetting angle θ_b at the corner edges described by Figure 3a are given by eq 2:

$$R = \frac{h}{2}\frac{1}{\sin\left(90° - \theta_b - \frac{\phi}{2}\right)} \tag{2}$$

where h is the arc length, θ_b is the wetting angle of the liquid, and ϕ is the corner angle of the edge. The Concus and Finn[25] condition derived from eq 2 assumes that $\theta_b < 90° - \phi/2$, so that capillary-driven flow may occur in the corner due to the decrease in the radius of curvature at the edge where two surfaces intersect. This condition describes mechanisms responsible for water transport in tall trees through hollow cells with a polygonal

(23) Brackbill, J. U.; Kothe, D. B.; Zemach, C. *J. Comput. Phys.* **1992**, *100*, 335.

(24) Adamson, A. W. *Physical Chemistry of Surfaces*, 5th ed.; John Wiley: New York, 1990; pp 4−10.

(25) Concus, P.; Finn, R. *Proc. Natl. Acad. Sci. U.S.A.* **1969**, *63*, 292.

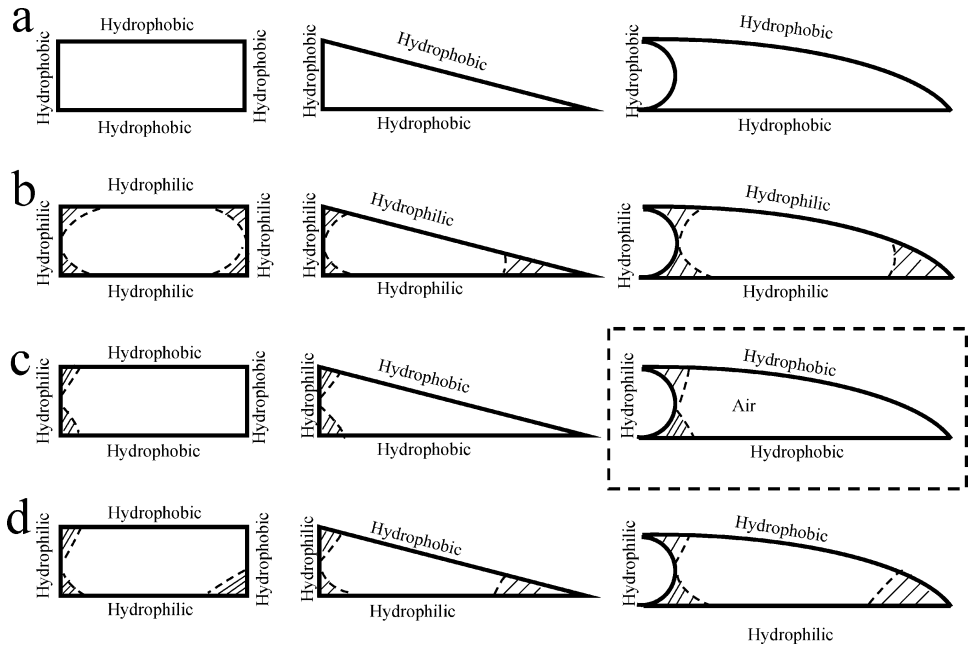

Figure 2. Schematic illustration of the wetting behaviors of a liquid (i.e., water, shaded areas) at corner edges of three different types of microchannels (rectangular, triangular, and elliptical) with various configurations of surface wettability. Hydrophobic refers to contact angle of 90° or higher. Hydrophilic corresponds to less than 45°: (a) all surfaces hydrophobic; (b) all surfaces hydrophilic; (c) one surface is hydrophilic, while the others are hydrophobic; and (d) adjacent surfaces either hydrophilic or hydrophobic. (Drawings are not to scale.)

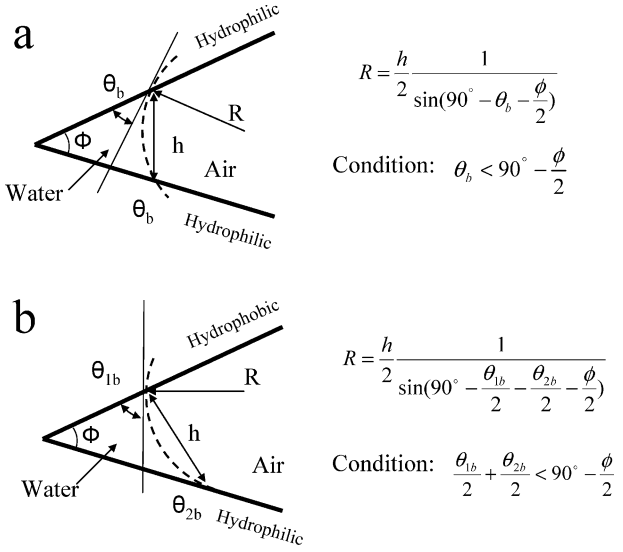

Figure 3. Schematic illustration of the wetting interface and radius of curvature of a liquid (water) at a corner in contact with (a) two hydrophilic wetting edges, and (b) a hydrophobic wetting edge adjacent to a hydrophilic one characterized by two different contact angles θ_{1b} and θ_{2b}.

cross-section conduit as well as the behavior of capillary surfaces in microgravity.[25] Hydrophilic wetting of corner edges requires a microchannel with $\theta_b < 90° - \phi/2$. We apply this condition to predict the liquid wetting and spreading behaviors at corners with arbitrary surface wettability.

When walls of the microchannels are hydrophobic (contact angle $\theta_b > 90°$) (Figure 2a), initial wetting and spreading of water at corner edges does not occur because wetting is not energetically favored. Wetting and spreading of liquid along corner edges occurs when the walls are hydrophilic ($\theta_b < 45°$) (Figure 2b). A smaller corner angle ϕ (as in the case of triangular and elliptical channels) is more easily wetted because a small wetting angle is not required to meet the Concus and Finn condition of eq 2.

A large corner angle with hydrophilic walls ($\theta_b < 45°$) that satisfies the condition $\theta_b + \phi/2 > 90°$ may represent a wetting liquid that can no longer spread along the corner edges; however, formation of a "spherical edge blob" is possible near the entrance of the microchannel.[26] A wetting liquid's spreading advance, or the inhibition of liquid spreading along corner edges of a microchannel, is the result of capillary pressure gradients due to the imbalance of capillary pressure, as reported by Dong and Chatzis,[27] and Dong et al.[28]

When a hydrophobic wetting edge is placed adjacent to a hydrophilic one (Figure 2c and d), corner wetting and spreading may occur as long as the condition $\theta_{1b}/2 + \theta_{2b}/2 < 90° - \phi/2$ is met. This wetting curvature described by Figure 3b has a radius of curvature R that is now given by eq 3. The wetting angles of water in contact with two wetting wedges, θ_{1b} and θ_{2b}, together with the corner angle, ϕ, predict the wetting behavior at a corner.

$$R = \frac{h}{2}\frac{1}{\sin\left(90° - \frac{\theta_{1b}}{2} - \frac{\theta_{2b}}{2} - \frac{\phi}{2}\right)} \quad (3)$$

Simulation of Stagnant Liquid at a Corner with Different Contact Angles. The FLUENT simulations of corner wetting model experimentally observed microdevice behavior based on the corner edges of an elliptical microchannel with dimensions of 12 μm fiber (minor axis) and a 100 μm channel opening (major axis) (Figure 1d). Our fabricated microchannels varied from one device to the next with channel half-widths ranging from 100 to 120 μm. We used the width of 100 μm for the model. The physical parameters used in the FLUENT simulations are those of water at 20 °C and atmospheric pressure: liquid density = 1000 kg/m^3; viscosity = 0.001 Pa s; surface tension = 0.1 N/m. Depending on the hydrophobic and/or hydrophilic character

(26) Concus, P.; Finn, R. *Phys. Fluids* **1998**, *10*, 39.
(27) Dong, M.; Chatzis, I. *J. Colloid Interface Sci.* **1995**, *172*, 278.
(28) Dong, M.; Dullien, F. A.; Chatzis, I. *J. Colloid Interface Sci.* **1995**, *172*, 21.

Table 1. Boundary Conditions (i.e., Contact Angle for Surfaces) for Simulations Shown in Figure 4

figure	fiber surface	top surface (PDMS)	bottom surface (OTS wafer)
4b	5°	5°	5°
4c	150°	150°	150°
4d	5°	100°	110°
4e	5°	150°	150°
4f	5°	150°	150°

of adjacent surfaces, specific boundary conditions such as wetting angles θ_b at microchannel walls were chosen for each run (Table 1). We tested the effect due to a channel half-width of 48 μm and obtained similar results with respect to boundary layer formation. This further confirms that the regions of interest are the triangular intersections between fiber/OTS and fiber/PDMS.

The simulation begins by first patching the corner region (5 μm by 5 μm) with liquid (water), followed by transient tracking of liquid−air interface. A steady-state solution is usually reached within a few microseconds (μs) of elapsed time within the simulation.

Figure 4 illustrates subtle differences that occur in the shape of water that wets a corner consisting of two hydrophilic surfaces (Figure 4b) as compared to two hydrophobic surfaces (Figure 4c). The hydrophilic case gives a concave liquid layer, while the hydrophobic case gives a convex liquid layer. The water spreads out more when a hydrophobic surface is in close proximity to a hydrophilic one (Figure 4d and e). The spreading occurs because an imbalance in surface free energies produces a surface tension gradient. The liquid deforms and flows toward the hydrophilic surface so that the water achieves an energetically stable state.

The mechanism involving the spreading of a stagnant liquid provides insight into how the dynamic focusing of the liquid layer along the fiber takes place as it transitions from corner wetting to boundary layer formation. Figure 4f represents a time-sequence of the computational simulation of wetting behavior in the corners of an elliptically shaped microchannel with adjacent hydrophobic and hydrophilic surfaces and an aspect ratio of 1:8. We use this simulation to understand the mechanisms involving the spreading advance of the liquid layer as it climbs the wall of the hydrophilic glass fiber under a partial vacuum.

The climbing effect of the liquid layer along the glass fiber occurs before the spreading advance reaches the microchannel outlet as demonstrated previously.[4] Before simulation, the corner region (now 6 μm × 6 μm) is patched with liquid (water). The simulation shows how boundary layer formation along the fiber starts with the wetting of two corner edges of the elliptical channel (t = 0), followed by deformation of the liquid due to the hydrophobicity of the channel walls (t = 0.4, 0.8, and 1.5 μs). Once the liquid held in the two corners merges together, a boundary layer is formed.

Experimentally, the wetting of the top left and the bottom left corner is achieved through capillary action in the absence of a pressure gradient across the fiber length. When vacuum is applied at the device outlet, the wetting liquid at the top and bottom corner edges begins to merge and forms a stable air−liquid interface. This interface between the top and bottom walls of the microchannel is stable for the 10 min duration of the run as long as a constant partial vacuum is maintained at the outlet. This mechanism was confirmed by a press-fit device constructed from 10 mm long glass fiber (θ_b = 5°) placed on a PDMS surface (θ_b = 89−110°) and pressed on an OTS derivatized wafer (θ_b = 110°) to form hydrophilic (glass fiber) and hydrophobic (PDMS and OTS) surfaces in close proximity to each other. A 1 μL volume of deionized water was placed into the well on the slide

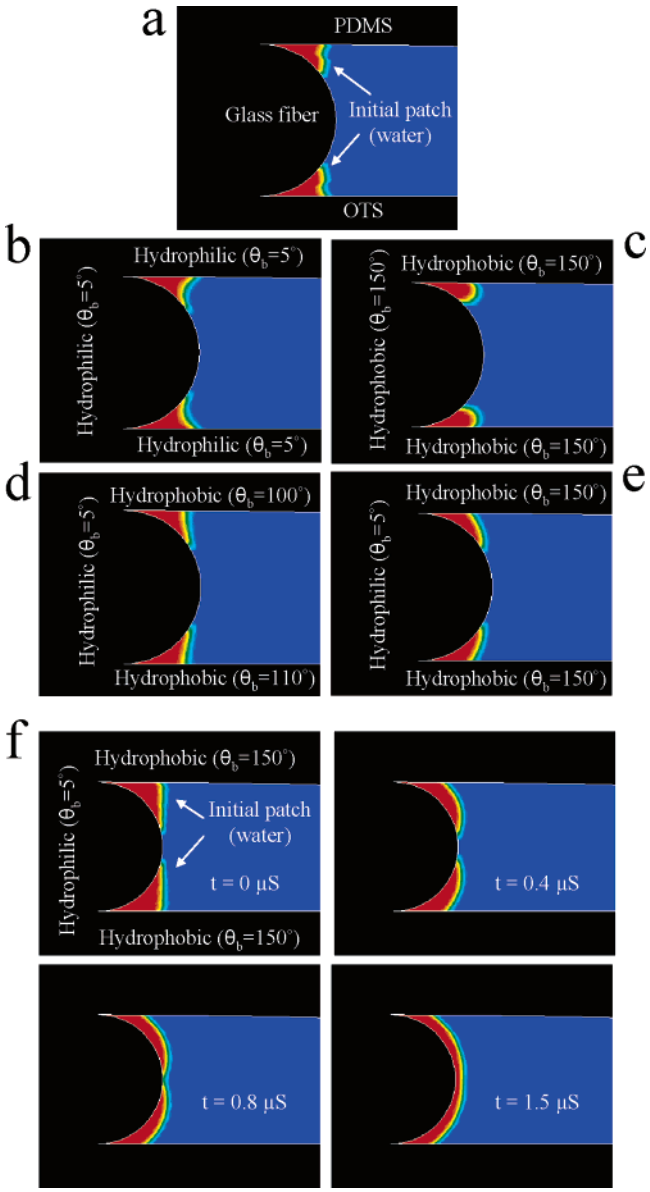

Figure 4. Simulation results of the expected wetting behaviors of an initially static liquid (water) at two corner edges of an elliptical microchannel with various predefined wetting angles. (Note the red regions indicate water, while the blue regions indicate air.) Boundary conditions for (b)−(e) are given in Table 1, while (f) is a time-sequence snapshot of wetting behavior at the corners. Width of channel from the center of the fiber to the edge is 100 μm, which results in an aspect ratio of approximately 8:1 (channel width to height (12 μm)).

and flowed through the device. Both visible light (Figure 5a,b) as well as confocal microscopy (Figure 1c) showed formation of a stable boundary layer whose characteristic thickness and width did not change during the 10 min duration of the run.

Stage 2: Stable Boundary Layer Flow. A pressure gradient parallel to the boundary layer draws a liquid from the well into the channel, and it initiates the movement of the liquid along the fiber and causes it to expand outward from the corner edges and partially fill the microchannel. The application of a pressure gradient produced by a positive pressure at the inlet or a partial vacuum at the outlet spreads the liquid along the length of the fiber and the corner edges. It facilitates the outward expansion of liquid from two corner edges. The air that is trapped in the channel touches three surfaces: PDMS, OTS, and the aqueous boundary layer next to the fiber. The surface activity of PDMS

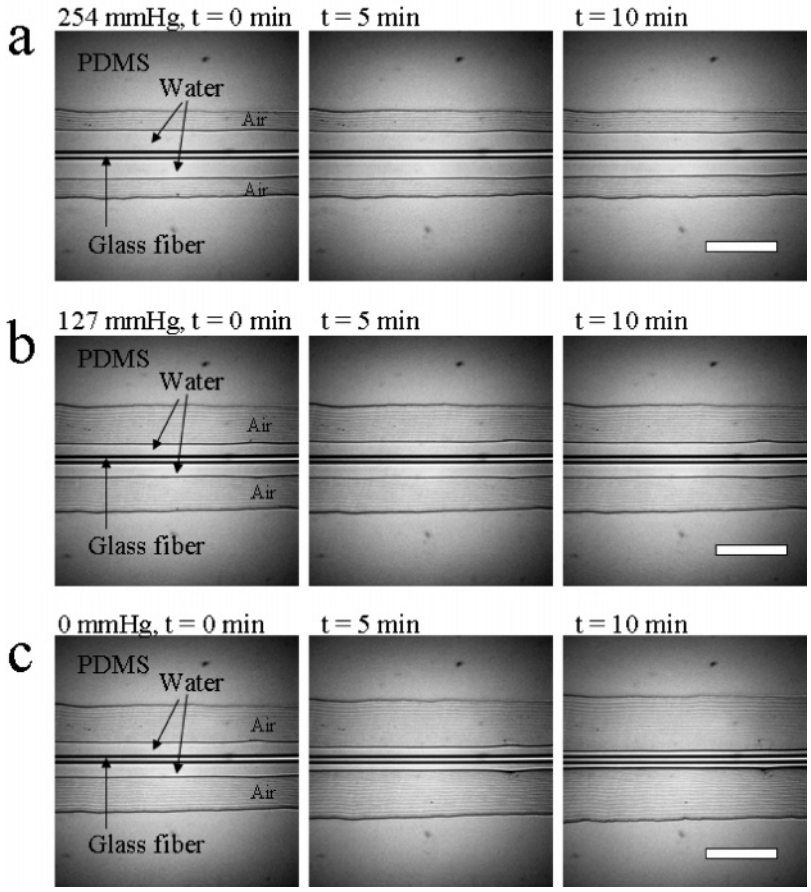

Figure 5. Photomicrograph showing boundary flow is stable for at least 10 min. A hydrophilic glass fiber 12 μm × 10 mm is sandwiched between hydrophobic PDMS and hydrophobic OTS-modified wafer. The center point of the fiber in the photomicrograph is at a distance of 5 mm, at a length/fiber diameter ratio of about 417. Water (1 μL) is placed in sample inlet and pulled into the microchannel from left to right under a constant vacuum with (a) at 254 mmHg, and (b) at 127 mmHg. A constant partial vacuum ensures a stable boundary layer flow for a duration of 10 min or longer. After the vacuum at the outlet is reduced to 0 mmHg from 127 mmHg, the boundary layer retracts back inward as seen in (c). When vacuum is again applied, flow occurs and the boundary layer returns to its original thickness (scale bar is 100 μm).

and OTS channel walls prevents the liquid from completely wetting the channel and focuses the liquid stream along the hydrophilic glass fiber.

The resulting boundary layer that forms next to the fiber (Figure 6) may also be explained by the Young−Laplace equation (eq 1). Because the radius of curvature R_2 in the direction parallel to the boundary layer is infinite, eq 1 simplifies to $\Delta P = \gamma/R_1$. The pressure in the concave side (water) is now higher than the pressure in the convex side (air). The radius of curvature of the interface between air and water inside the microchannel promotes the stability of a boundary layer formed adjacent to hydrophobic surfaces in rectangular, triangular, and elliptical channels (Figure 7). From confocal images shown in Figure 1b and c, the channel geometry and boundary layer under vacuum are similar to what is illustrated in Figure 6d, and to a lesser degree, that illustrated in Figure 6b and c.

Effect of Channel Geometry and Contact Angles on Meniscus Shape. The radius of curvature of the wetting meniscus R_R depends on channel geometry and contact angles. Equation 4 gives R_R as a function of channel height h and wetting angles θ_{1b} and θ_{2b} for a rectangular channel (Figure 7a). A hydrophobic wetting interface is formed when $\cos\theta_{1b} + \cos\theta_{2b} < 0$.

$$R_R = \frac{-h}{\cos\theta_{1b} + \cos\theta_{2b}} \tag{4}$$

where h is the channel height, and θ_{1b} and θ_{2b} are the wetting angles of the liquid in contact with two parallel wetting edges. For a triangular-shaped channel, the radius of curvature R_T depends on the triangle's corner angle ϕ, as shown in eq 5:

$$R_T = \frac{h}{2}\frac{1}{\sin\left(\frac{\theta_{1b}}{2} + \frac{\theta_{2b}}{2} - 90° - \frac{\phi}{2}\right)} \tag{5}$$

The arc length of the meniscus, h, due to hydrophobic-directed wetting between two walls, the wetting angles of the liquid, θ_{1b} and θ_{1b}, in contact with two wetting edges, a corner, and the corner angle of the triangle, ϕ, is illustrated in Figure 7b. For a triangle with height a, and width b, the corner angle ϕ and arc length h are given by eqs 6 and 7. The condition for hydrophobic wetting is now $\theta_{1b}/2 + \theta_{2b}/2 > 90° + \phi/2$. Hence, for a PDMS surface with a contact angle of 100° and an OTS surface with a contact angle of 110°, the condition predicts a corner angle ϕ that cannot be greater than 30° to maintain a stable hydrophobic wetting interface. As predicted by this condition, there is a discontinuous transition in wetting behavior at the crossing point where $\theta_{1b}/2 + \theta_{2b}/2 = 90° + \phi/2$ (or $\phi = 30°$). When $\theta_{1b}/2 + \theta_{2b}/2 < 90° + \phi/2$ (or $\phi > 30°$), a hydrophobic wetting curvature cannot be stably maintained and the water layer will spread out.

$$\phi = \arctan\left(\frac{b}{a}\right) \tag{6}$$

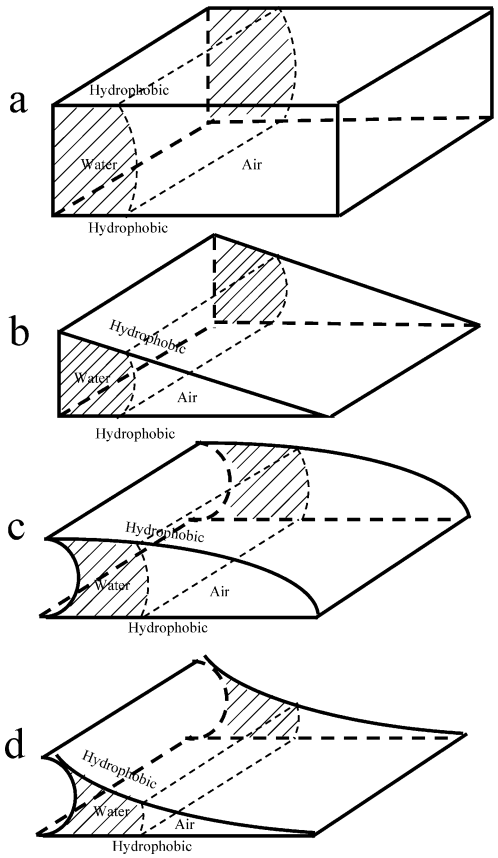

Figure 6. Schematic three-dimensional illustration of the focused liquid inside four different types of microchannels: (a) rectangular, (b) triangular, (c) elliptical, and (d) elliptical with rotational symmetry from (c). (Drawings are not to scale.)

where b is the height and a is the width.

$$h = \left[b - \frac{bx}{a}\right] \frac{1}{\cos\left(\frac{-\theta_{1b} + \theta_{2b} + \phi}{2}\right)} \tag{7}$$

Equation 5 also gives the radius of curvature R_E for an elliptical channel with angle ϕ and length h, defined by eqs 8 and 9. Because ϕ is the angle between the horizontal axis and tangent line of the ellipse (Figure 7c), it is a function of a and b, the length of two principal vertices of the eclipse, and x the distance between origin ($x = 0$) measured from the center of the fiber and liquid layer. The radius, R_E, decreases as the wetting interface moves away from the origin ($x = 0$) to the corner edge of the microchannel ($x = a$), and ϕ varies from 0° at $x = 0$ to 90° at $x = a$, where a denotes the half-width of the microchannel.

The corner angle ϕ is given by:

$$\phi = \arctan\left(\frac{b}{a} \frac{1}{\sqrt{\left(\frac{a}{x}\right)^2 - 1}}\right) \tag{8}$$

where a and b are the two principal vertices of ellipse, and x is the distance from interface on a from the center.

$$h = \left[b\sqrt{1 - \left(\frac{x}{a}\right)^2}\right] \frac{1}{\cos\left(\frac{-\theta_{1b} + \theta_{2b} + \phi}{2}\right)} \tag{9}$$

where a and b are the two principal vertices of ellipse and x is the distance of wetting interface on a from the center. ϕ is the corner angle described by eq 8.

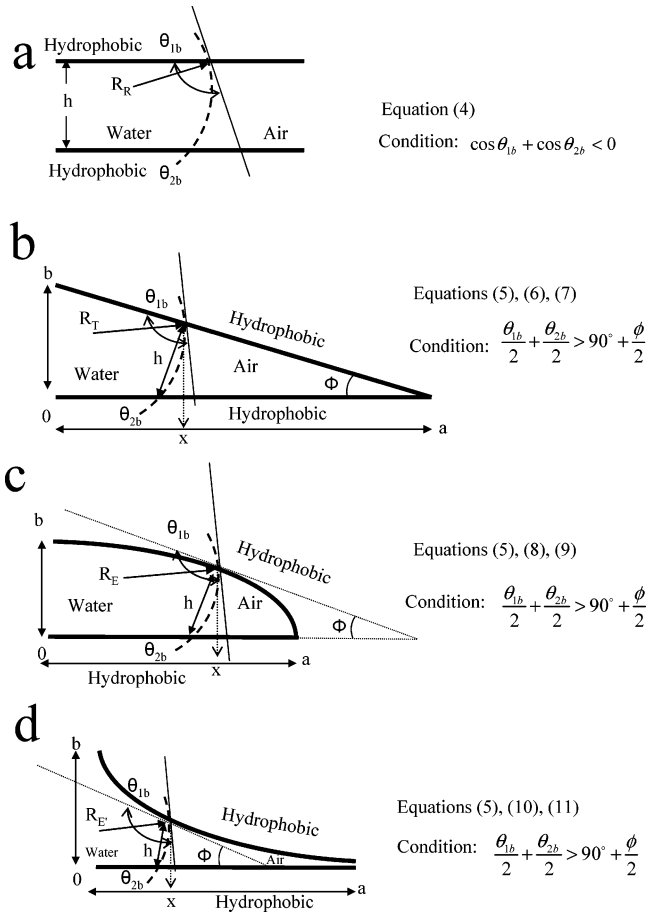

Figure 7. Schematic illustration of the wetting curvature (dotted line) and the radii of curvature of a liquid (water) in contact with two hydrophobic walls that have two different contact angles θ_{1b} and θ_{2b}. Four different types of microchannels are shown: (a) rectangular, (b) triangular, (c) elliptical, and (d) elliptical with rotational symmetry from (c).

For the case where the rotational symmetry is used to describe an elliptical channel (Figure 7d), the radius of curvature ($R_{E'}$) is also given by eq 5. However, the ϕ and h are now given by eqs 10 and 11.

$$\phi = \arctan\left(\frac{b}{a} \frac{1}{\sqrt{\left(\frac{a}{a - x}\right)^2 - 1}}\right) \tag{10}$$

$$h = \left[b - b\sqrt{1 - \frac{(a - x)^2}{a^2}}\right] \frac{1}{\cos\left(\frac{-\theta_{1b} + \theta_{2b} + \phi}{2}\right)} \tag{11}$$

In general, for the rectangular microchannel, the radius of curvature R_R of the liquid−air interface is constant along the width of the channel. There exists a critical pressure P_{max} ($P_{max} = \Delta P = \gamma/R_1$)[11,12] over which the pressure at the liquid (water) side is larger, and the liquid breaches the liquid−air interface so that the channel fills with liquid. For the case of press-fit elliptical microchannels, the radius of curvature for the liquid−air interfaces varies with the width of the channels and is largest near the glass fiber and smallest at the edges. A larger P_{max} is expected if the air−liquid interface is located near the corner edge.

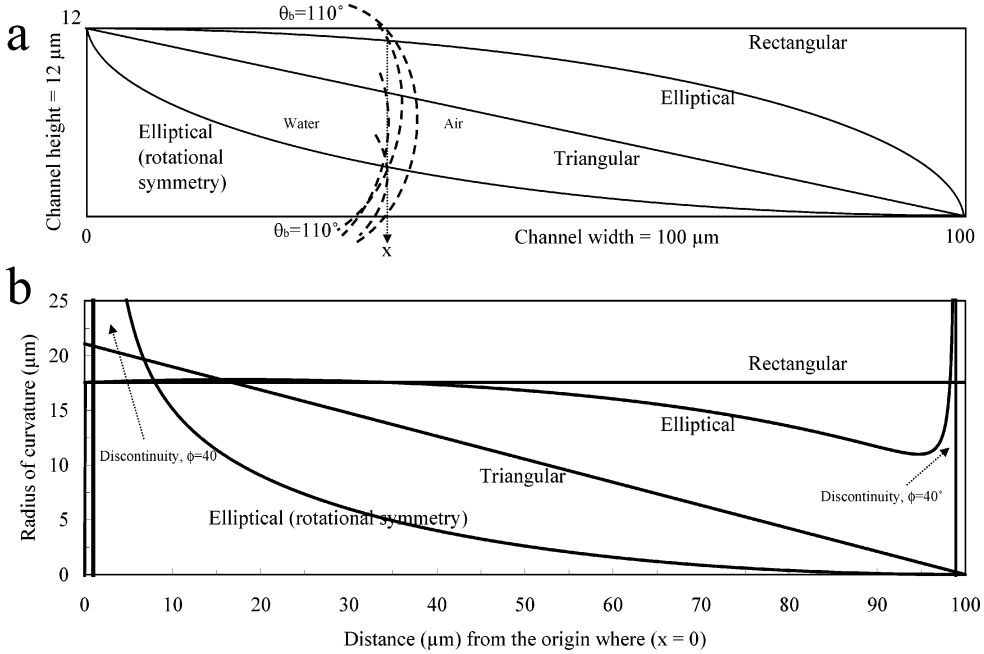

Figure 8. (a) Schematic illustration showing the microchannel dimensions superimposed with four types of channel geometries (rectangular, elliptical, triangular, and elliptical with rotational symmetry). All four geometries are constrained with the same channel height (12 μm) and width (100 μm). Four wetting menisci (dotted lines) in contact with the top and bottom walls of the channels are shown at a distance x away from the origin (where $x = 0$). The wetting angle θ_b is 110°. The variations in radius of curvature of the wetting meniscus along the width of the channel are shown in (b). The radii of curvature (R) were calculated using eqs 4−11, where $a = 100$ μm, $b = 12$ μm, and $\theta_b = \theta_{1b} = \theta_{2b} = 110°$.

Water (surface tension = 0.1 N/m at room temperature), with a radius of curvature of 5 μm at the interface, requires an overpressure of 2×10^4 Pa[1] 0.2 atm, or 152 mmHg[2] to obtain wetting. This means a hydrophobic corner with small radius of curvature does not wet easily and the geometry of a microchannel is extremely important in maintaining a stable boundary layer flow. In general, maintaining such flow in a hydrophobic rectangular-shaped microchannel (Figure 6a) is more difficult when compared to an elliptical (Figure 6c and d) or triangular-shaped channel (Figure 6b).

The wetting meniscus radius of curvature variation along the width of different channel types shown in Figure 8 summarizes our explanation. All four geometries illustrated in Figure 7 have the same channel height ($b = 12$ μm), width ($a = 100$ μm), and wetting angle ($\theta_b = 110°$) as summarized in Figure 8a. For each geometry, the radius of curvature of the wetting interface may be calculated along the width of the channel using eqs 4−11. Because the wetting angle θ_b is the same for parallel or adjacent wetting edges, θ_{1b} and θ_{2b} are replaced by θ_b where $\theta_{1b} = \theta_{2b} = \theta_b = 110°$.

The rectangular channel has a constant radius of curvature that equals 17.5 μm and a critical pressure (P_{max}) of 0.056 atm (Figure 8b). The elliptical channel (rotational symmetry case) has a radius of curvature of 4.9 μm (Figure 8b). The P_{max} is 0.201 atm with a boundary width of 35 μm. This analysis shows an elliptically or triangularly shaped microchannel can tolerate a much larger overpressure due to the smaller radius of curvature at the hydrophobic corners with low corner angles. This provides an environment favorable to a stable boundary layer where the liquid is always effectively pinned at the center location near and adjacent to the fiber of the channel. A balance between the pressure of the boundary layer and the critical pressure, P_{max}, is found at this location, which translates into a stable boundary layer.

At the conditions given above, a microchannel with triangular geometry has a corner angle $\phi = 6.8°$. For two elliptical geometries, ϕ varies from 0° to 90° along the width of the channel. The condition ($\theta_{1b}/2 + \theta_{2b}/2 > 90° + \phi/2$) predicts a discontinuity behavior at $\phi = 40°$ where the condition $\theta_{1b}/2 + \theta_{2b}/2 = 90° + \phi/2$ is reached. This is of particular interest because, at this point, a small change in either wetting angle or corner angle can result in a large discontinuous transition in wetting behavior. Such is the case where the condition $\theta_{1b}/2 + \theta_{2b}/2 < 90° + \phi/2$ is reached. By increasing ϕ to a value larger than 40°, the equilibrium wetting configuration characterized by a hydrophobic wetting curvature can suddenly change discontinuously, and possibly transition into a hydrophilic wetting curvature where the water layer spontaneously spreads out.

Summary of Mechanisms. Two mechanisms have been identified to explain the experimentally observed and mathematically simulated wetting phenomena in a microchannel where geometry and surface chemistry control the wetting. The first mechanism, corner wetting, is based on the close proximity of a hydrophobic (PDMS or OTS) surface and hydrophilic surface (glass fiber) at the corner edge. These surfaces work together to produce a net surface tension force that deforms and then fuses the liquid at the two corner edges into a thin boundary layer. The second mechanism, wall wetting, describes whether liquid flow from wetted corners establishes itself as a stable boundary layer flow or as a channel filling flow. The fluid boundary layer seeks the lowest energetic state and expands through corner wetting into corner edges that define the upper and lower parts of the channel. The hydrophobicity of the PDMS and OTS and the curvature of the PDMS surface prevent outward expansion, and therefore stably focus the liquid boundary layer along the hydrophilic glass fiber. Unlike triangular or elliptical channels, rectangular channels have a constant radius of curvature and a constant liquid−air interfacial area across the cross-section of the channel; therefore, surface forces are insufficient to constrain the boundary layer and the rectangular channel fills with liquid.

Conclusions

We demonstrate liquid−air boundary layer formation in a fluidic microchannel device constructed from a hydrophilic glass microfiber and two hydrophobic surfaces (a flexible PDMS film, and an inflexible glass or SiO_2 wafer). This configuration forms channels of semi-elliptical cross-section that direct water to a boundary layer next to a glass fiber, which serves to guide and center liquid flow in the middle of the channel. We employed the Young−Laplace equation to develop a model that explains how these boundary layers form in microfluidic channels. Model simulations using FLUENT were compared to experimental results and showed good agreement. These expressions permit material surface contact angle to be combined with microfluidic channel geometry and fluid properties to predict the microfluidic devices' boundary layer flow characteristics. This has advanced our understanding of fluid flow in microfluidic channels with a liquid−static air boundary layer and the application of surface free energy to direct boundary layer fluid flow in these channels. Together with our facile device assembly method, the model will enable new types of microfluidic devices to be built to predetermined flow and path specification where channel flow characteristics are directed by the surface chemistry control within the microchannel.

Acknowledgment. This research was supported through a Cooperative Agreement with the Agricultural Research Service of USDA (Grant #1935-42000-035), a grant from National Defense University (Contract #DABJ29-03-P-0022), Purdue University Agricultural Research Programs, and the Birck Nanotechnology Center of Discovery Park at Purdue University. K.S.L. was supported by the ERC for Advanced Bioseparation Technology, KOSEF, Korea. We thank Jennifer Sturgis and J. Paul Robinson at the Purdue University Cytometry Lab for confocal microscopy and other access to their imaging facility. We also thank Jennifer Sturgis for the creative idea of using a microscope glass cover slip as a surface for the microchannel as a means to achieve better confocal images. We thank Dr. Jim Leary and Youngmi Kim of Purdue University for internal review of this paper, and Dr. Jim Leary for suggesting the concept that this technique may be effective in the hydrodynamic focusing of cells.

Supporting Information Available: FLUENT volume of fluids (VOF) mathematical models. This material is available free of charge via the Internet at http://pubs.acs.org.

LA053465H